Dysregulation of Grainyhead-like 3 expression causes widespread developmental defects

Zihao Deng
Monash University
Tariq Butt
Monash University
Benedicta D. Arhatari
La Trobe University
Charbel Darido
Peter MacCallum Cancer Centre
Alana Auden
Monash University
Dijina Swaroop
Monash University
Darren D. Partridge
Monash University
Katharina Haigh
University of Manitoba
Thao Nguyen
Monash University
Jody J. Haigh
University of Manitoba
Marina R. Carpinelli
Monash University
Stephen Jane (stephen.jane@monash.edu)
Monash University

Research Article

Keywords: Grhl3, transcription factor, GRHL3, neural tube defects (NTDs), bacterial artificial chromosome (BAC)

Posted Date: September 16th, 2021

DOI: https://doi.org/10.21203/rs.3.rs-885196/v1

Abstract

The gene encoding the transcription factor, Grainyhead-like 3 (*Grhl3*), plays critical roles in mammalian development and homeostasis, and these have been uncovered through analysis of loss-of-function models. *Grhl3*-null embryos exhibit a range of gross phenotypes including a shortened longitudinal axis, thoraco-lumbo-sacral spina bifida and soft-tissue syndactyly. Additional studies reveal that these embryos also exhibit a proliferation/differentiation imbalance in the epidermis. This manifests as a failure in skin barrier formation resulting in peri-natal lethality, and defective wound repair. Conditional inactivation of *Grhl3* in the squamous epithelium of adult skin, head and neck tissues, and oesophagus reproduces this proliferation/differentiation imbalance and leads to squamous cell carcinomas. These observations establish GRHL3 as a critical tumour suppressor. Despite these extensive analyses of *Grhl3* loss-of-function models, the consequences of gain-of-function of this gene have been difficult to achieve. We have redressed this issue through the generation of a novel mouse model that expresses *Grhl3* from a transgene integrated in the *Rosa26* locus on an endogenous *Grhl3*-null background. Expression of the transgene rescues both the neurulation and skin barrier defects of the knockout mice, allowing survival into adulthood. Despite this, the mice are not normal, exhibiting a range of phenotypes attributable to dysregulated *Grhl3* expression. In mice homozygous for the transgene, we observe a severe Shaker-Waltzer phenotype associated with hearing impairment. Micro-CT scanning of the cochleae and the vestibular apparatus revealed profound structural alterations underlying these phenotypes. In addition, these mice exhibit other developmental anomalies including hair loss, digit defects and epidermal dysmorphogenesis. These findings indicate that diverse developmental processes display low tolerance to dysregulation of *Grhl3*.

Introduction

Grainyhead-like 3 (*Grhl3*), is a member of a family of mammalian transcription factors descended from the *Drosophila* grainyhead (*grh*) gene[1–3]. During murine embryogenesis, *Grhl3* is predominantly expressed in the surface ectoderm from embryonic day (E) 8.5[4]. Expression is also observed along the E8.5 neural plate border from which the otic placode arises from the pre-placodal region, and in the inner and outer hair cell of the cochlea[4–7]. *Grhl3* plays critical roles in mammalian development and homeostasis that have been uncovered through analysis of loss-of-function models. Constitutive gene inactivation in embryogenesis leads to a failure of caudal neural tube closure, which manifests as thoraco-lumbo-sacral spina bifida – a major subtype of neural tube defects (NTDs), and a hypomorphic *Grhl3* allele has been identified as the underlying defect in the curly tail (*ct*) mouse strain, a model of neural tube closure for more than 70 years[8,9]. *Grhl3*-null embryos also exhibit soft-tissue syndactyly, and a shortened anterior-posterior axis due to defects in the planar cell polarity signaling pathway[5,10,11]. The latter also manifests as defective wound healing and perturbed stereociliary bundles in the inner ear[5,10]. Newborn *Grhl3*-null mice die soon after birth of dehydration due to a failure of the skin barrier to form, and exhibit a marked disruption in keratinocyte differentiation and impaired epidermal architecture[10,12–15]. In the adult, conditional inactivation of *Grhl3* in the squamous epithelial tissues of

the skin and head and neck reproduces this proliferation/differentiation imbalance and leads to squamous cell carcinoma, establishing *Grhl3* as a critical tumour suppressor at these sites[14,16]. In humans, mutations in *GRHL3* are associated with Van der Woude syndrome that is characterised by cleft palate, and are recognised as a major predisposing factor for spina bifida[17–19]. Multiple *de novo* and inherited variants have been reported in patients with NTDs[18,19].

To date, only one mouse over-expression model utilising a bacterial artificial chromosome (BAC) containing *Grhl3* has been reported[20]. In this study, ~ 1.5 to 2-fold over-expression of *Grhl3* was associated with spina bifida[20]. In zebrafish, over-expression of *Grhl3* through micro-injection of full length *Grhl3* mRNA into the 1–2 cell stage embryos yielded axial defects but not NTDs[21]. In the current study, we established and characterised a novel mouse model of *Grhl3* misexpression. In contrast to the previous study[20], we did not identify NTDs in transgenic mice with *Grhl3* over-expression, but identified multiple other developmental defects, emphasising the need for stringent regulation of this gene during murine embryogenesis.

Results

Restoration of Grhl3 expression in Grhl3-knockout mice rescues skin barrier and neural tube defects

We and others have previously attempted to generate mouse lines over-expressing *Grhl3* using a wide variety of regulatory elements to drive expression, including the keratin (*K*)-14, *CAG*, and B6 (*CMV*) promoters ([22] and unpublished data). Despite multiple rounds of injections, we never identified any pups expressing the transgene, suggesting that over-expression of *Grhl3* is incompatible with embryonic survival. This was subsequently affirmed, with *Grhl3* transgenic embryos shown to undergo growth arrest and death at E5.5[22]. To redress this, we devised a strategy to express a *Flag-Grhl3* transgene on a *Grhl3*-null background. The transgene was inserted into the murine *Rosa26* locus, allowing expression of *Flag-Grhl3* from the *Rosa26* regulatory elements (*Rosa26*^{Tg}, Supplementary Fig. S1)[23]. Tissue- and temporal-specificity was achieved through deletion of a *loxP-STOP-loxP* cassette in the *Rosa26* locus immediately upstream of the *Flag-Grhl3* coding region that was induced by an intercross of the *Rosa26*$^{Tg/Tg}$ line with a line in which the *Cre* recombinase gene had been knocked into the endogenous *Grhl3* locus, rendering *Cre*-positive mice *Grhl3*-heterozygotes (Supplementary Fig. S1)[24]. Further crosses generated offspring that were null at the endogenous locus (*Grhl3*$^{Cre/Cre}$) and heterozygous or homozygous for the transgene (Supplementary Fig. S1). Intact transgene knock-in was confirmed by Sanger DNA sequencing (data not shown), and deletion of the *loxP-STOP-loxP* cassette was confirmed by PCR analysis (Supplementary Fig. S1). Dissection of uteri from *Grhl3*$^{Cre/+}$;*Rosa26*$^{Tg/+}$ intercrosses at E18.5 frequently showed litters of three to four embryos (expected litter size average 6.5 embryos[25]), with a high number of resorptions. Genotyping of 237 offspring showed that wild-type embryos (WT - *Grhl3*$^{+/+}$;*Rosa26*$^{+/+}$), embryos heterozygous for the *Grhl3-Cre* allele or the transgene or both (*Grhl3*$^{Cre/+}$;*Rosa26*$^{+/+}$, *Grhl3*$^{+/+}$;*Rosa26*$^{Tg/+}$,

Grhl3$^{Cre/+}$;*Rosa26*$^{Tg/+}$), and embryos homozygous for the *Grhl3-Cre* allele (*Grhl3*$^{Cre/Cre}$;*Rosa26*$^{Tg/+}$, *Grhl3*$^{Cre/Cre}$;*Rosa26*$^{+/+}$) were present at the predicted Mendelian ratios, whereas under-representation of embryos carrying two alleles of the *Grhl3* transgene (*Grhl3*$^{+/+}$;*Rosa26*$^{Tg/Tg}$, *Grhl3*$^{Cre/+}$;*Rosa26*$^{Tg/Tg}$ and *Grhl3*$^{Cre/Cre}$;*Rosa26*$^{Tg/Tg}$) was observed (Table 1). Surprisingly, this under-representation was not dependent on the presence of a *Cre* allele.

Table 1
Expected and observed numbers of embryos carrying corresponding genotypes from the intercross of *Grhl3*$^{Cre/+}$;*Rosa26*$^{Tg/+}$ mice at E18.5. Expected numbers of embryos were calculated as average litter size of 6.5 embryos. A one sample χ^2 test was used for data analysis. P-values are for comparison between the expected and observed number of embryos. * = P-value < 0.05.

Genotype	Expected number of embryos	Observed number of embryos	P-value
Grhl3$^{+/+}$;*Rosa26*$^{+/+}$	18.28	25	0.12
Grhl3$^{Cre/+}$;*Rosa26*$^{+/+}$	36.56	36	0.93
Grhl3$^{Cre/Cre}$;*Rosa26*$^{+/+}$	18.28	17	0.76
Grhl3$^{+/+}$;*Rosa26*$^{Tg/+}$	36.56	36	0.93
Grhl3$^{Cre/+}$;*Rosa26*$^{Tg/+}$	73.13	68	0.55
Grhl3$^{Cre/Cre}$;*Rosa26*$^{Tg/+}$	36.56	33	0.56
Grhl3$^{+/+}$;*Rosa26*$^{Tg/Tg}$	18.28	5	**0.002***
Grhl3$^{Cre/+}$;*Rosa26*$^{Tg/Tg}$	36.56	9	**< 0.00001***
Grhl3$^{Cre/Cre}$;*Rosa26*$^{Tg/Tg}$	18.28	8	**0.016***
Total number from 45 litters	292.5	237	**0.001***

To assess the level of *Grhl3* expression, we isolated epidermis from E18.5 embryos and performed quantitative reverse transcription PCR (Q-RT-PCR) analyses using primer pairs that would selectively amplify endogenous *Grhl3*, transgene-derived *Grhl3*, or both. As expected, no endogenous *Grhl3* mRNA was detected in any embryos genotyped as *Grhl3*$^{Cre/Cre}$, and no transgene expression was seen in *Rosa26*$^{+/+}$ embryos (Fig. 1A-C). Embryos heterozygous for both endogenous *Grhl3* and the transgene (*Grhl3*$^{Cre/+}$;*Rosa26*$^{Tg/+}$), and embryos carrying a single copy of the transgene in the absence of endogenous *Grhl3* (*Grhl3*$^{Cre/Cre}$;*Rosa26*$^{Tg/+}$), had expression levels equivalent to WT embryos (Fig. 1A). Embryos homozygous for the transgene and homozygous or heterozygous for endogenous *Grhl3* (*Grhl3*$^{Cre/+}$;*Rosa26*$^{Tg/Tg}$ and *Grhl3*$^{Cre/Cre}$;*Rosa26*$^{Tg/Tg}$) exhibited an approximately 2-2.5-fold increase in total *Grhl3* mRNA levels compared to WT (Fig. 1A). Attempts at quantitation of transgene expression by

immunoblotting with an anti-FLAG antibody were unsuccessful (data not shown), possibly due to protein folding obscuring the N-terminal FLAG epitope.

As identified in our previous studies[10], inactivation of both endogenous *Grhl3* alleles (as seen in *Grhl3*$^{Cre/Cre}$;*Rosa26*$^{+/+}$embryos), leads to a profound skin barrier defect, as evidenced by penetration of the externally delivered dye, toluidine blue (Fig. 2B)[26], with WT embryos excluding the dye (Fig. 2A). The *Grhl3*$^{Cre/Cre}$;*Rosa26*$^{+/+}$ embryos further mimicked the *Grhl3*$^{-/-}$ mice, displaying fully penetrant thoraco-lumbo-sacral spina bifida, curly tail, open eyelids, round body shape and a short longitudinal embryonic axis (Fig. 2B). *Grhl3*$^{Cre/Cre}$;*Rosa26*$^{+/+}$ embryos also showed oedematous limbs, with soft-tissue syndactyly (Fig. 2E-G), and died soon after birth, phenocopying the *Grhl3*$^{-/-}$ embryos[10,11,20]. Rescue of the skin barrier defect was observed in *Grhl3*$^{Cre/Cre}$;*Rosa26*$^{Tg/+}$ embryos, indicative of functional GRHL3 protein derived from the transgene in these animals (Fig. 2C). Spina bifida was also rescued in these mice, although a shortened longitudinal axis and residual curly tail was observed, suggesting that functional GRHL3 protein levels in this context were approximately 30% of WT (and similar to the *curly tail* strain). NTDs were fully rescued in mice carrying two copies of the transgene (*Grhl3*$^{Cre/Cre}$;*Rosa26*$^{Tg/Tg}$), as was the skin barrier defect (Fig. 2D), indicating that over-expression of *Grhl3* is compatible with normal neural tube closure and epidermal barrier function. One novel developmental consequence of *Grhl3* over-expression was observed, with 50% of the *Grhl3*$^{Cre/Cre}$;*Rosa26*$^{Tg/Tg}$ embryos displaying synpolydactyly, with incomplete digit formation, indicating impaired digit patterning and morphogenesis (Fig. 2E-G). This was also observed with lower penetrance in the *Grhl3*$^{Cre/Cre}$;*Rosa26*$^{Tg/+}$ embryos (9%), suggesting a dose response (Fig. 2G).

Restoration of Grhl3 expression in Grhl3-knockout mice partially rescues epidermal differentiation

We next examined the epidermal architecture in the various mouse lines at E18.5 using hematoxylin and eosin (H&E) staining and immunohistochemistry (IHC) analysis with proliferative and cell differentiation markers. Consistent with our previous findings in *Grhl3*-null embryos[10,14], *Grhl3*$^{Cre/Cre}$;*Rosa26*$^{+/+}$ embryos displayed a markedly thicker epidermis compared to WT embryos (Fig. 3). The stratum corneum (SC) layer of *Grhl3*$^{Cre/Cre}$;*Rosa26*$^{+/+}$ epidermis was compacted, and both the stratum granulosum (SG) and stratum spinosum (SP) layers were expanded. In addition, *Grhl3*$^{Cre/Cre}$;*Rosa26*$^{+/+}$ stratum basale (SB) appeared disorganised in its cellular arrangement (Fig. 3). Interestingly, we noticed an extra tissue structure residing superiorly to the SC of *Grhl3*$^{Cre/Cre}$;*Rosa26*$^{+/+}$ epidermis. This structure contained an underlying anucleate layer, attached to the SC, and a superior layer of nucleated cells (Fig. 3). Kashgari, et al. [11] have recently identified that GRHL3 is necessary for periderm morphogenesis and non-adhesive function as digits separate. We postulate that this extra tissue structure may result from periderm dysmorphogenesis due to inactivation of *Grhl3*. Despite its normal barrier function, the epidermal architecture of *Grhl3*$^{Cre/Cre}$;*Rosa26*$^{Tg/+}$ embryos reassembled that of *Grhl3*$^{Cre/Cre}$;*Rosa26*$^{+/+}$ epidermis, but

without the extra tissue structure (Fig. 3). *Grhl3*$^{Cre/+}$;*Rosa26*$^{Tg/+}$, *Grhl3*$^{Cre/+}$;*Rosa26*$^{Tg/Tg}$ and *Grhl3*$^{Cre/Cre}$;*Rosa26*$^{Tg/Tg}$ epidermis exhibited a normal morphological appearance (Fig. 3).

IHC analysis of various cell differentiation markers on E18.5 epidermis showed that the expression domain of the basal marker, K5, was expanded into layers above the SB of the *Grhl3*$^{Cre/Cre}$;*Rosa26*$^{+/+}$ epidermis. K5 expression in *Grhl3*$^{Cre/Cre}$;*Rosa26*$^{Tg/+}$, *Grhl3*$^{Cre/+}$;*Rosa26*$^{Tg/+}$, *Grhl3*$^{Cre/+}$;*Rosa26*$^{Tg/Tg}$ and *Grhl3*$^{Cre/Cre}$;*Rosa26*$^{Tg/Tg}$ epidermis resembled the WT control (Fig. 3). Similar normalisation of expression was seen with the terminal differentiation markers loricrin and filaggrin, and the suprabasal marker K1 in *Grhl3*$^{Cre/Cre}$;*Rosa26*$^{Tg/+}$, *Grhl3*$^{Cre/+}$;*Rosa26*$^{Tg/+}$, *Grhl3*$^{Cre/+}$;*Rosa26*$^{Tg/Tg}$ and *Grhl3*$^{Cre/Cre}$;*Rosa26*$^{Tg/Tg}$ embryos compared with the *Grhl3*$^{Cre/Cre}$;*Rosa26*$^{+/+}$ epidermis, indicating that restoration of *Grhl3* expression largely redressed the differentiation defects that are the hallmark of *Grhl3*-null epidermis. Positive staining with all four of these markers was observed in the extra tissue layer above the SC in the *Grhl3*$^{Cre/Cre}$;*Rosa26*$^{+/+}$ epidermis. This observation suggests that the extra tissue layer contained differentiating cells. Only K6, a marker of epidermal repair, was mildly up-regulated in the *Grhl3*$^{Cre/Cre}$;*Rosa26*$^{Tg/+}$ and *Grhl3*$^{Cre/+}$;*Rosa26*$^{Tg/+}$ epidermis compared to WT (Fig. 3), but expression of this marker was markedly lower than in *Grhl3*$^{Cre/Cre}$;*Rosa26*$^{+/+}$ epidermis. Consistent with normalisation of differentiation markers and barrier function in embryos expressing endogenous or transgene-derived GRHL3, Transglutaminase 1 (*Tgm1*), a direct GRHL3 target gene critical for epidermal barrier formation[10,27], was expressed in epidermis from the *Grhl3*$^{Cre/+}$;*Rosa26*$^{Tg/Tg}$, *Grhl3*$^{Cre/+}$;*Rosa26*$^{Tg/+}$, *Grhl3*$^{Cre/Cre}$;*Rosa26*$^{Tg/+}$ and *Grhl3*$^{Cre/Cre}$;*Rosa26*$^{Tg/Tg}$ embryos (Supplementary Fig. S2).

We then examined the expression of the proliferation marker, PCNA, in E18.5 transgenic epidermis. PCNA-positive cells were widely distributed in both basal and suprabasal layers in the *Grhl3*$^{Cre/Cre}$;*Rosa26*$^{+/+}$ and *Grhl3*$^{Cre/Cre}$;*Rosa26*$^{Tg/Tg}$ epidermis with more than 80% of epidermal cells being PCNA-positive in the latter, indicating keratinocyte hyperproliferation (Fig. 4A, B). The *Grhl3*$^{Cre/Cre}$;*Rosa26*$^{Tg/+}$ and *Grhl3*$^{Cre/+}$;*Rosa26*$^{Tg/Tg}$ epidermis also showed significantly higher percentage of PCNA-positive cells compared to WT (Fig. 4A, B). In contrast, PCNA positivity in the *Grhl3*$^{Cre/+}$;*Rosa26*$^{Tg/+}$ epidermis did not differ from the WT control (Fig. 4A, B).

Over-expression of Grhl3 perturbs epidermal homeostasis in adult mice

To explore the consequences of *Grhl3* over-expression, we followed the progress of ageing *Grhl3*$^{Cre/+}$;*Rosa26*$^{Tg/Tg}$ and *Grhl3*$^{Cre/Cre}$;*Rosa26*$^{Tg/Tg}$ mice, which we had shown previously were the two genotypes with excess total *Grhl3* expression compared to WT mice (Fig. 1A). We observed severe alopecia in the dorsal region and tails of mice of both genotypes (Fig. 5A). H&E staining of hair follicles showed evident clefts between the inner root sheath (IRS) and the outer root sheath (ORS) of the *Grhl3*$^{Cre/+}$;*Rosa26*$^{Tg/Tg}$ and *Grhl3*$^{Cre/Cre}$;*Rosa26*$^{Tg/Tg}$ adult mice but not in age-matched WT controls (Fig. 5B). This finding was reminiscent of the *Grhl1*-knockout adult mice, which exhibit regional hair loss

with grooming, due to loss of expression of its direct target gene Desmoglein-1a (*Dsg1a*), a desmosome component important for hair shaft anchorage[28]. Q-RT-PCR analysis of the epidermis showed comparable levels of *Grhl1* and *Dsg1a* expression in *Grhl3*$^{Cre/+}$;*Rosa26*$^{Tg/Tg}$ and *Grhl3*$^{Cre/Cre}$;*Rosa26*$^{Tg/Tg}$ mice and WT controls (Supplementary Fig. S2), suggesting that alternate mechanisms underlie alopecia mediated by *Grhl3* over-expression.

H&E staining showed no difference in epidermal architecture between WT, *Grhl3*$^{Cre/+}$;*Rosa26*$^{Tg/Tg}$ and *Grhl3*$^{Cre/Cre}$;*Rosa26*$^{Tg/Tg}$ adult epidermis (Fig. 5C). Expression patterns of K5, K14, loricrin and involucrin were also comparable between WT, *Grhl3*$^{Cre/+}$;*Rosa26*$^{Tg/Tg}$ and *Grhl3*$^{Cre/Cre}$;*Rosa26*$^{Tg/Tg}$ epidermis (Fig. 5C). However, there was a very subtle elevation of K6 expression in the adult *Grhl3*$^{Cre/+}$;*Rosa26*$^{Tg/Tg}$ and *Grhl3*$^{Cre/Cre}$;*Rosa26*$^{Tg/Tg}$ epidermis, whereas no K6 expression was detected in WT adult epidermis (Fig. 5C). These findings indicate that normal *Grhl3* expression in the epidermis is also necessary for epidermal hemostasis during postnatal life.

Examination of PCNA expression revealed a well-organised lining of PCNA-positive cells, largely confined to the SB layer of WT epidermis. In contrast, PCNA expression in both the *Grhl3*$^{Cre/+}$;*Rosa26*$^{Tg/Tg}$, and the *Grhl3*$^{Cre/Cre}$;*Rosa26*$^{Tg/Tg}$ epidermis was not confined to the basal layer, with PCNA-positive cells visible in the suprabasal regions, and highly disorganised in their arrangement (Fig. 5C). Quantification of the staining identified less than 35% PCNA-positive cells in WT epidermis, while around 60% cells were PCNA-positive in adult *Grhl3*$^{Cre/Cre}$;*Rosa26*$^{Tg/Tg}$ epidermis and 43% in *Grhl3*$^{Cre/+}$;*Rosa26*$^{Tg/Tg}$ adult epidermis (Fig. 5D). These observations were consistent with findings in the embryonic epidermis, demonstrating that over-expression of *Grhl3* promotes hyperproliferation of basal keratinocytes in adult epidermis.

Over-expression of Grhl3 leads to inner ear malformation and hearing impairment

We noticed that adult mice over-expressing *Grhl3* displayed several behavioral abnormalities, including hyperactivity, poor balance, high-speed bidirectional circling, head bobbing and head tilting (Supplementary Fig. S3). These abnormalities are collectively referred to as the Shaker-Waltzer phenotype and are typically associated with inner ear vestibular dysfunction[29]. To further investigate the correlation between *Grhl3* misexpression and the Shaker-Waltzer phenotype, we quantified the circling behaviours of adult transgenic mice. *Grhl3*$^{Cre/Cre}$;*Rosa26*$^{Tg/Tg}$ mice performed more than 80 revolutions per minute on average, whereas *Grhl3*$^{Cre/+}$;*Rosa26*$^{Tg/Tg}$ mice circled around 40 times per minute (Fig. 6A). In contrast, WT mice showed no circling behaviour (Fig. 6A). We previously showed that *Grhl3*$^{+/-}$;*Vangl2*$^{+/-}$ mice exhibited disordered orientation of stereociliary bundles on the sensory hair cells in the cochlea, due to disruption of the PCP pathway[5]. Therefore, we sought to investigate whether the Shaker-Waltzer phenotype resulted from cochlear hair cell misorientation. This was not the case, with cochlear phalloidin staining showing well-organised inner and outer hair cells on cochlear basilar membrane of newborns aged between postnatal day 1 to 7 (Supplementary Fig. S4).

Given the normal stereociliary morphology, we postulated that Shaker-Waltzer phenotype may originate from structural defects of the inner ear. We therefore visualised this structure using micro-computed tomography (μCT) scanning. The μCT analysis was performed with the vestibular labyrinth and cochlea enclosed by the auditory bulla to minimise structural damage, followed by a 3D reconstruction to provide clearer images of the internal structure. The WT inner ear exhibited structural integrity of lateral, posterior and anterior semi-circular canals, ampullae, and cochlea. In contrast, the posterior and anterior semi-circular canals of the *Grhl3*$^{Cre/Cre}$;*Rosa26*$^{Tg/+}$ inner ear were completely truncated, and the lateral semi-circular canals were grossly enlarged compared to WT (Fig. 6B). The ampullae in these mice were also enlarged or absent, and the cochleae were strikingly larger in size compared to WT but with a relatively intact structurally (Fig. 6B). The *Grhl3*$^{Cre/Cre}$;*Rosa26*$^{Tg/Tg}$ inner ear was totally deformed, with bulbous cochleae lacking structural definition, and mostly absent or truncated semi-circular canals and ampullae (Fig. 6B). As *Grhl3*$^{Cre/Cre}$;*Rosa26*$^{+/+}$ embryos died soon after birth, we examined the E18.5 skeletal preparations of the temporal bones. The *Grhl3*$^{Cre/Cre}$;*Rosa26*$^{+/+}$ inner ear showed normal morphological appearance that resembled the WT controls (Supplementary Fig. S4). These observations indicate that *Grhl3* misexpression compromises inner ear morphogenesis and leads to Shaker-Waltzer phenotype.

To identify if inner ear malformation leads to hearing impairment, we performed an auditory brainstem response (ABR) test to assess the hearing capacity of transgenic mice. In this test, the ABR threshold, which is the quietest sound that elicits an ABR, is similar to the hearing threshold[30]. Commensurate with the inner ear malformations, the ABR test revealed significant hearing impairment in *Grhl3*-over-expressing mice compared to WT controls (Fig. 6C, D), with the average ABR threshold of WT mice at 26 decibel sound pressure level (dB SPL), compared to 59 dB SPL in *Grhl3*$^{Cre/Cre}$;*Rosa26*$^{Tg/+}$ mice and 85 dB SPL in *Grhl3*$^{Cre/Cre}$;*Rosa26*$^{Tg/Tg}$ mice when responding to mixed frequency noise. At the single frequency level, hearing impairment was most significant in *Grhl3*$^{Cre/Cre}$;*Rosa26*$^{Tg/Tg}$ mice when responding to 4 kHz, 8 kHz, 16 kHz and 32 kHz pure tone stimuli, but *Grhl3*$^{Cre/+}$;*Rosa26*$^{Tg/Tg}$ mice also showed a severe hearing impairment (Fig. 6D). Moreover, the overall average ABR threshold across different genotypes also displayed a stepwise increase with a threshold shift at around 6–10 dB SPL in *Grhl3*$^{Cre/+}$;*Rosa26*$^{Tg/+}$ mice, 20–30 dB SPL in *Grhl3*$^{Cre/+}$;*Rosa26*$^{Tg/Tg}$ mice, 25–35 dB SPL in *Grhl3*$^{Cre/Cre}$;*Rosa26*$^{Tg/+}$ mice, and at 48–64 dB SPL in *Grhl3*$^{Cre/Cre}$;*Rosa26*$^{Tg/Tg}$ mice (Fig. 6D). Importantly, the shape and width of click-evoked ABR peaks were normal in all tested mice (Supplementary Fig. S5), indicating that hearing impairment in transgenic mice resulted from ear defects rather than abnormality of the vestibulocochlear nerve or brainstem.

Discussion

In this study, we have for the first time successfully over-expressed *Grhl3* in adult mice, allowing us to uncover previously unsuspected developmental events that are dependent on stringent regulation of GRHL3. We achieved this using a *Grhl3*-null allele (*Grhl3*^{Cre}) to induce expression of a *Grhl3* transgene inserted into the murine *Rosa26* locus. Mice homozygous for the null allele (*Grhl3*$^{Cre/Cre}$) and lacking

transgene expression exhibited the classic defects described in the original *Grhl3* constitutive knockout[8], of neural tube defects, short longitudinal body axis, failure of the skin barrier to form and peri-natal lethality. These defects were completely rescued in mice carrying two copies of the *Rosa26*-based transgene, with the animals surviving to adulthood. However, multiple novel phenotypic abnormalities were observed as a consequence of dysregulated *Grhl3* expression, with digit defects, impaired epidermal homeostasis with alopecia, the Shaker-Waltzer phenotype, hearing impairment, and inner ear malformations all evident.

De Castro, et al. [20] reported the first successful attempt of over-expressing *Grhl3* in late-stage mouse embryos, utilising the hypomorphic *curly tail* strain to generate the line[9]. *Grhl3* expression was driven by a bacterial artificial chromosome (BAC), encompassing the endogenous *Grhl3* locus. A ~ 1.5 to 2-fold increase in total *Grhl3* mRNA expression above WT levels was documented in the caudal region of E9.5 and E10.5 embryos and a less then 1.2-fold increase in the epidermis of E18.5 embryos that were double homozygotes for $Grhl3^{ct}$ allele and the BAC transgene ($Grhl3^{ct/ct;TgGrhl3/TgGrhl3}$). Interestingly, 67% of these embryos displayed NTDs, a phenotype we never observed in our transgenic embryos, despite comparable levels of *Grhl3* over-expression. None of the De Castro, et al. [20] embryos displayed digit defects or abnormal epidermal morphology, and phenotypes in adult mice were not reported. The phenotypic discrepancies between the two lines, particularly the NTDs, cannot be attributed to differences in the initial timing, location or magnitude of expression of *Grhl3*. Both lines restricted expression to tissues that usually express *Grhl3* at the appropriate developmental time-point; De Castro, et al. [20] through use of the endogenous locus in a BAC, and our line via *Cre* expression from the endogenous locus activating the transgene. However, several other differences may underlie the phenotypic discrepancies. Firstly, *Grhl3* once over-expressed in our line would remain so, as the *Rosa26* locus lacks any endogenous regulatory elements that are retained in the BAC, and may influence *Grhl3* expression. Secondly, and in our view more likely, *Grhl3* mRNA and protein is derived from a cDNA construct in our transgene, whereas it is derived from the endogenous locus in the BAC. Several studies have highlighted the importance of intronic RNA for *GRHL3* regulation[31–33], particularly in the context of epidermal differentiation[31]. Lack of intronic elements in our transgenic embryos may lead to further dysregulation of *Grhl3* expression. This implies that correct regulation of *Grhl3* expression is crucial for embryonic development of multiple systems. Similarly, over-expression of *Grhl3* has previously been shown to induce different developmental consequences in different models[20,21].

A surprising finding in our model, was the under-representation of embryos homozygous for the transgene (irrespective of the presence or absence of a *Cre* allele), suggesting that “leaky” expression of the transgene in early embryogenesis had dire developmental consequences. This finding is in keeping with the previous reports on the $Actb^{Cre};CAG^{LSL-Grhl3}$ mouse line, which displayed early lethality at E5.5[22]. We postulate that this may result from random transmission of Cre recombinase from the sperm to the oocyte where the unexpected deletion of the upstream *loxP-STOP-loxP* sequence of the transgene occurred even if the consequential embryos are *Cre* ‘negative’ genetically[34], or the inheritance of *delta* allele (activated transgene allele) by the offspring due to germline recombination occurred during

gametogenesis in male *Grhl3*$^{Cre/+}$;*Rosa26*$^{Tg/+}$ mice[35], leading to certain level of *Grhl3* expression that is incompatible with early embryonic survival. Therefore, surviving homozygous transgenic mice presumably had faithful transgene expression, that commenced only after *Grhl3-Cre* was activated at E8.5. This is consistent with our PCR and Q-RT-PCR analyses showing no deletion of the *loxP-STOP-loxP* cassette, or *Grhl3* transgene expression, in E18.5 *Grhl3*$^{+/+}$;*Rosa26*$^{Tg/Tg}$ embryos.

In *Grhl3*$^{Cre/Cre}$;*Rosa26*$^{Tg/Tg}$ embryos, transgene-mediated expression of *Grhl3* fully rescued the epidermal barrier defect, and largely normalised keratinocyte terminal differentiation in both embryos and adult mice. Surprisingly, it did not correct basal cell hyperproliferation and expansion. Previous studies have shown that diverse mechanisms centred on reducing *Grhl3* RNA levels are critical for maintaining low levels of GRHL3 protein expression in epidermal stem cells, thereby preventing differentiation[31,33]. Consistent with this, constitutive *Grhl3*-knockout mice display failed epidermal differentiation associated with expansion of a proliferative stem cell pool[10,12,14]. Therefore, the persistence of a hyperproliferative and expanded basal layer, despite normal differentiation shown here, would suggest that it is not simply the level of *Grhl3* mRNA that is important for epidermal stem cell behaviour. In keeping with this, hyperproliferation in the *Grhl3*$^{Cre/Cre}$;*Rosa26*$^{Tg/+}$ epidermis was far greater than in *Grhl3*$^{Cre/+}$;*Rosa26*$^{Tg/+}$ epidermis, despite both lines having comparable total *Grhl3* mRNA levels. Similarly, *Grhl3*$^{Cre/+}$;*Rosa26*$^{Tg/Tg}$ mice exhibited less basal cell proliferation than *Grhl3*$^{Cre/Cre}$;*Rosa26*$^{Tg/Tg}$ mice despite slightly higher levels of total *Grhl3* expression. These findings suggest that either the endogenous transcript is important for stem cell homeostasis, or that higher levels of transgene expression are deleterious to stem cell behaviour.

Another unexpected skin phenotype, severe alopecia, was also observed as a consequence of *Grhl3* over-expression. Our previous studies in adult conditional *Grhl3*-knockout mice revealed no alopecia[27], whereas both *Grhl3*$^{Cre/Cre}$;*Rosa26*$^{Tg/Tg}$ and *Grhl3*$^{Cre/+}$;*Rosa26*$^{Tg/Tg}$ mice displayed dorsal hair loss that mimicked the grooming alopecia phenotype we had previously observed in constitutive *Grhl1*-knockout mice[28]. In that line, alopecia was due to poor hair anchorage as a result of detachment of the IRS from the ORS, due to loss of expression of the GRHL1 target gene, *Dsg1a*. Neither *Grhl1* nor *Dsg1a* levels were altered in the *Grhl3* over-expressing lines compared to WT, suggesting that the hair anchorage phenotype may be due to perturbed expression of other Desmoglein genes[36,37]. As this phenotype was more severe in mice with higher levels of transgene expression, and given the complete absence of a comparable phenotype in adult *Grhl3* conditional knockout mice[27], it is unlikely that the presence of the endogenous transcript exerts any influence on hair anchorage.

Although GRHL1 deficiency causes inner ear malformation in zebrafish, and *GRHL2* has been identified as an autosomal-dominant deafness gene in humans, *Grhl3* has not previously been linked to inner ear structural defects or hearing impairment[38–40]. Our previous research had identified a key role for *Grhl3* with *Vangl2* in planar cell polarity mediated orientation of cochlear hair cell stereocilia[5]. Here, we found that misexpression of *Grhl3* had no impact on cochlear hair cell orientation, but did result in severe bony labyrinth dysmorphogenesis. Normally, the semi-circular canals provide sensory input for rotary

movement, with the end of each canal extending into an ampulla in which hair cells excite the afferent fibre of the vestibular nerve upon head and body movement[41,42]. The lateral and superior canals detect the movement in vertical axis and lateral axis respectively, and structural defects result in head tilting in mice. The posterior canal detects movement in left-right axis and defects result in circling behaviour in mice[41,42]. The transgenic mice displayed vestibular disturbance, and a Shaker-Waltzer phenotype that mirrored the degree of severity of the ampulla and semi-circular canal malformation. The ABR test also revealed a positive correlation between hearing impairment and the severity of inner ear structural defects. Interestingly, severity was again linked to the levels of expression of the transgene rather than total *Grhl3* mRNA levels, with $Grhl3^{Cre/Cre}$;$Rosa26^{Tg/+}$ mice more severely afflicted than $Grhl3^{Cre/+}$;$Rosa26^{Tg/+}$ animals. Given that the $Grhl3^{Cre/Cre}$;$Rosa26^{+/+}$ inner ear showed normal morphological appearance, it appears that the levels of expression of the transgene rather than loss of the endogenous transcript is detrimental to inner ear development.

A recent study identified that intron 1 of the nascent human *GRHL3* RNA provides binding sites for the Cleavage and Polyadenylation Specificity Factor (CPSF) complex and HNRNPA3. This suppresses exonic splicing and promotes intronic polyadenylation, lowering GRHL3 expression and preventing the premature differentiation of primary human keratinocytes[31]. In humans, four alternatively spliced isoforms of *GRHL3* have been characterised[2,17,43]. Although no murine *Grhl3* splice isoforms have been discovered to date, it is likely that *Grhl3* alternative splicing is conserved in mouse to generate transcript variants[44]. Early in embryonic development, the precursor of the inner ear, the otic placode, is derived from the pre-placodal region (PPR), located in the territory of the neural plate border[7,45]. Notably, expression of the PPR marker, *Six1*, overlaps with *Grhl3* spatiotemporally in mouse embryos[6,46]. We propose that the cDNA-based *Grhl3* transgene may induce abnormal differentiation of the PPR and consequently, inner ear defects and hearing impairment. This may indicate that a specific *Grhl3* mRNA isoform allows this process to occur, and expression of the incorrect splice isoform from the transgene perturbs inner ear development.

In conclusion, our study has highlighted that stringent regulation of *Grhl3* expression is an absolute requirement for numerous developmental processes. In particular, epidermal differentiation and hair anchorage, digit formation, and formation of the cochlea and vestibular apparatus are affected. In addition, it has raised the concept that not only are the levels of the transcription factor important, but also that isoform-specific roles may govern different morphogenetic events.

Materials And Methods

Mice

To misexpress *Grhl3*, a *Flag-Grhl3* transgene preceded by a floxed transcriptional stop sequence ($Rosa26^{Tg}$) was activated by *Grhl3* knock-in-*Cre* ($Grhl3^{Cre}$). This generated a mouse ($Grhl3^{Cre}$;$Rosa26^{Tg}$) that express FLAG-GRHL3 in place of endogenous GRHL3. The $Rosa26^{Tg}$ mouse line was generated as

described previously[23]. Briefly, a *Grhl3* cDNA-containing pENTR1A construct and a pRMCE DV1 destination vector were amalgamated into a single targeting vector through Gateway LR Clonase II (Thermo Fisher Scientific)-mediated *in vitro* recombination. The mouse *Grhl3* cDNA was generated as previously described[8]. The targeting vector was then introduced into the Recombinase Mediated Cassette Exchange (RMCE)-compatible murine G4 ROSALUC embryonic stem cells (ESCs) by electroporation. Insertion into the *Rosa26* locus occurred through a FLPe-mediated RMCE. Positive clones were selected based upon 5' PCR using a combination of external (forward 5'-AAA GCT CTG AGT TGT TAT-3') and internal (reverse 5'-GCG GCC TCGACT CTA CGA TA-3') primers at the site of 5' integration and on restored neomycin resistance. Positive ESC clones were aggregated with CD1 diploid host embryos and strong chimeras bred for germline transmission of the $Rosa26^{Tg}$ targeted allele[47]. $Grhl3^{Cre}$ mice[24] were crossed with $Rosa26^{Tg/Tg}$ mice and $Grhl3^{Cre/+}$;$Rosa26^{Tg/+}$ offspring were intercrossed through timed mating overnight. Deletion of the floxed transcriptional stop sequence was confirmed by PCR using genomic DNA isolated from E18.5 epidermis with the following primers: *floxed* forward (5'-GAG GAC AAA CTC TTC GCG GT-3'), *floxed* reverse (5'-CAG AGG CTG CTG ATC TCG TT-3'), *delta* reverse (5'-TAT CCG CTT CTC CTT GGG AC-3'). The PCR product size of the *floxed* allele is 631 bp and of the *delta* allele is 492 bp. All the experimental animals were maintained under a mixed background. The gestational age of embryos was identified as E0.5 at midday on the day of detection of a vaginal plug. All the animal experiments were approved by the Alfred Research Alliance Animal Ethics Committee with project number E/1900/2019/M. Research was conducted in the accordance of the Australian Code for the Care and Use of Animals for Scientific Purposes and the Australian Code for the Responsible Conduct of Research and in compliance with the ARRIVE guidelines.

Genotyping of mice

Mice were genotyped using genomic DNA isolated from tails biopsies or yolk sacs by PCR. The *Grhl3* knock-in-*Cre* allele was genotyped using the following primers: *Grhl3KI-Cre* forward (5'-CAC CCC CTC AGC TAA GAA GGA A-3'), *Grhl3KI-Cre* WT reverse (5'-CCC TTT GGC AAG AGG AGA GAA A-3') and *Grhl3KI-Cre* KI reverse (5'-TCC CTG AAC ATG TCC ATC AGG T-3'). The PCR product size of the WT allele is 702 bp and of the *Cre* allele is 420 bp. *Grhl3* transgene at the *Rosa26* locus was genotyped using the following primers: *Rosa26* 5' (5'-AAA GTC GCT CTG AGT TGT TAT-3'), *Rosa26* WT 3' (5'-GGA GCG GGA GAA ATG GAT ATG-3') and *Rosa26* MUT 3' (5'-GCG AAG AGT TTG TCC TCA ACC-3'). The PCR product size of the WT allele is 600 bp and of the *Grhl3* transgene on *Rosa26* allele is 300 bp.

Skin barrier assay and skeletal preparation

For skin barrier assay, embryos were fixed in methanol on a roller mixer for 5 min and then washed in PBS twice for 5 min. Fixed embryos were incubated in 0.1% (w/v) toluidine blue for 5 minutes, then washed, imaged and stored in PBS at 4°C. Skeletal preparations were performed as previously described[48]. Images of embryos and skeletal preparation were obtained using Nikon SMZ1500 stereomicroscope with AxioVision software (Zeiss).

Histology and immunohistochemistry

For histological analysis, skin samples were fixed in 4% (w/v) PFA for at least 24 hrs at room temperature. Samples were then processed using a Leica ASP300S and embedded into paraffin. Samples were sectioned in a transverse orientation at 5 µm thickness and collected onto SuperFrost plus slides (Thermo Fisher Scientific). Hematoxylin and eosin (H&E) staining was performed using standard methods. Immunohistochemistry (IHC) was performed as per standard protocols using 3,3'-diaminobenzidine (DAB) staining (Vector Laboratories) or Mouse on Mouse immunodetection (Vector Laboratories). Images of sections were obtained using Nikon ECLIPSE Ci-L upright microscope with NIS-Elements D software, then analysed and quantified using ImageJ software and GraphPad Prism 8. Antibodies used for IHC were anti-Keratin 1 (Covance, PRB-149P-100, 1:500, 45 min, RT), anti-Filaggrin (Covance, PRB-417P-100, 1:1000, 45 min, RT), anti-Loricrin (Covance, PRB-145P-100, 1:500, overnight, 4°C), anti-Involucrin (Covance, PRB-140C, 1:750, 10 min, RT), anti-Keratin 5 (Covance, PRB-160P, 1:500, 45 min, RT), anti-Keratin 14 (Covance, PRB-155P, 1:1000, 45 min, RT), anti-Keratin 6 (Covance, PRB-169P-100, 1:500, 45 min, RT), anti-PCNA (CST, 2586, 1:2000, 30 min, RT) and goat anti-rabbit secondary antibody (Vector Laboratories, ZB0318, 1:200, 30 min, RT).

Phalloidin staining and confocal microscopy

To access hair cells, firstly, bony labyrinth was dissected from mice at the age of postnatal one to six days. Secondly, cochlea was opened and the spiral ligament and its attached organ of Corti were separated from cochleae. Thirdly, organ of Corti was separated from the spiral ligament. Finally, the hair cell-containing sensory epithelia were separated from the spiral limbus of organ of Corti and fixed in 4% (w/v) PFA at 4°C for at least 24 hrs. Hair cell Phalloidin staining was performed as previously described[5]. Samples were imaged using a Nikon Eclipse Ti inverted A1R confocal microscope through a CFI Apochromat TIRF 60× Oil objective. 15 to 30 images spaced 0.5 µm apart were collected by NIS-Elements Advanced Research software. The images were then analysed by ImageJ software.

Mice behavioral examination and auditory brainstem response test

An individual mouse was placed in a single cage. Physical activities within 1 min were recorded using a Canon EOS 60D camera. Circling behaviour was quantified by manual counting and analysed using GraphPad Prism 8. For auditory brainstem response (ABR) test, mice were anaesthetised through intraperitoneal injection of anesthetic mixture (100 mg/kg ketamine, 50 mg/kg xylazine and 30 mg/kg acepromazine). Mice eyes were covered by lubricating eye ointment (Poly Visc, Alcon) to avoid desiccation and body temperature was maintained with a 37°C heating pad. Anesthesia was confirmed by the absence of the pedal reflex. ABR test was performed using an evoked potential workstation (Tucker Davis Technologies). Briefly, an anaesthetised mouse was placed inside a Faraday cage, with a free-field magnetic speaker installed 10 cm from the left pinna. The Faraday cage was contained by a sound attenuation chamber. A 100 µsec click with a frequency between 0 to 50 kHz and a set of 3 msec pure tone stimuli at 4, 8, 16 and 32 kHz were delivered with maximum intensities of 100 dB SPL. ABRs were detected using 3 subdermal electrodes (Rochester Electro-Medical): the positive electrode was deposited at the vertex of the skull; the negative electrode was positioned in the left cheek and the ground electrode

was placed at the hind left leg. Through the positive electrode, the auditory evoked potential can be extracted from the neural electrical activity and transformed into waveforms. BioSig software (Tucker Davis Technologies) was used to determine the ABR threshold by averaging collected ABRs over 512 repetitions of each stimulus. The lowest consistent ABR-evoking intensity stimulus was identified as the threshold.

X-ray micro-computed tomography

Adult mice were sacrificed and the inner ear containing auditory bulla was dissected from the petrous part of the temporal bone as previously described[49]. Samples were fixed in 10% (v/v) neutral buffered formalin (NBF) at room temperature. X-ray micro-computed tomography (μCT) scanning was performed using an Xradia MicroXCT-200 (Carl Zeiss X-ray Microscopy) as described[50]. Three-dimensional (3D) reconstructed images were obtained and segmented using Avizo-6.2 software (Mercury Computer Systems). 3D modelling and following analyses were performed in blinded to genotypes.

Reverse transcription and quantitative polymerase chain reaction

Mice dorsal skin samples were harvested, and snap froze in liquid nitrogen. Epidermis was separated from the skin by incubating with 1 mg/mL dispase in PBS at 4°C overnight. Epidermis was then homogenized in TRIsure (Bioline) and RNA was isolated according to the manufacturer's instructions. RNA was then treated by a TURBO DNA-free kit (Invitrogen) to remove genomic DNA and reverse transcribed using a Transcriptor First Strand cDNA Synthesis Kit (Roche). Quantitative reverse transcription PCR (Q-RT-PCR) was performed using GoTaq qPCR master mix (Promega) on a LightCycler 480 Instrument (Roche). Relative expression values were generated using the ΔΔCT method by standardising genes of interest to *Actb* and analysed using GraphPad Prism 8. Oligonucleotide primers used for Q-RT-PCR were *Grhl3* endogenous & transgene forward (5'-CGA GGC CTG GAA GAC ATA CC-3'), *Grhl3* endogenous & transgene reverse (5'-CTC AGA GCA GCC ACA CTC TC-3'), *Grhl3* endogenous forward (5'-AGC CAA CCA GAG ACG GAT C-3'), *Grhl3* endogenous reverse (5'-AGG CCT CGT CCT CAT TAC TG-3'), *Grhl3* transgene forward (5'-ACA AGG ACG ACG ATG ACA AG-3'), *Grhl3* transgene reverse (5'-CCG TTG ACT CTC ATC ATG GC-3'), *Tgm1* forward (5'-CTC CTT CTG GGC TCG TTG TT-3'), *Tgm1* reverse (5'-ATT TAC ACC ACT GCC CCG AG-3'), *Grhl1* forward (5'-GCG CGA TGA CAC AGG AGT A-3'), *Grhl1* reverse (5'-GGA ACG ACT TCC AGG CTT CA-3'), *Dsg1a* forward (5'-GGG ATA ACC ACC ATC TGT GT-3'), *Dsg1a* reverse (5'-CCT CCC AGA TCT TGC ATT TC-3'), *Actb* forward (5'-GAT ATC GCT GCG CTG GTC GTC-3') and *Actb* reverse (5'-CAG CTC ATT GTA GAA GGT GTG G-3').

Statistical analysis

A one sample χ^2 test was used to compare the expected and observed numbers of E18.5 embryos, P-values were determined with 1 degree of freedom. Relative expression of genes, % of PCNA-positive cells in epidermis, number of mice revolutions per minute and average ABR thresholds were compared between wild-type and other genotypes using one-way ANOVA tests following by Dunnett's multiple

comparison tests with a GraphPad Prism 8 software. When comparing the total *Grhl3* mRNA abundance between wild-type and *Grhl3*$^{Cre/Cre}$;*Rosa26*$^{Tg/Tg}$ animals in Fig. 1A, an additional Mann-Whitney test was used with a GraphPad Prism 8 software.

Declarations

Acknowledgement

We would like to thank Karen Alt and Christina Makhlouf from the Australian Centre for Blood Diseases, Jacqueline Ogier from the Murdoch Children's Research Institute and Smitha Georgy from the University of Melbourne for their assistance. We also would like to acknowledge the outstanding technical services of the Murdoch Children's Research Institute, Monash Histology Platform, Monash Micro Imaging, Monash Animal Research Platform, Monash Micromon Genomics and Monash Biomedical Imaging.

Funding

This work was supported by the Australian National Health and Medical Research Council (project grant 1106434).

Author contributions

Z.D., C.D., M.R.C. and S.M.J. conceived the study and developed the methodology. C.D., K.H., J.J.H. and T.N. designed and generated the mouse line. Z.D., T.B., B.D.A., A.A., D.S., D.D.P and M.R.C. performed the experiments. Z.D., T.B., B.D.A., M.R.C. and S.M.J. analysed and interpreted the results. Z.D. and S.M.J wrote the manuscript. All authors revised and approved the final version of the manuscript.

Competing interests

The authors declare no competing interests.

References

1. Wilanowski, T. *et al.* A highly conserved novel family of mammalian developmental transcription factors related to Drosophila grainyhead. *Mech Dev*, **114**, 37–50 https://doi.org/10.1016/s0925-4773(02)00046-1 (2002).
2. Ting, S. B. *et al.* The identification and characterization of human Sister-of-Mammalian Grainyhead (SOM) expands the grainyhead-like family of developmental transcription factors. *Biochem J*, **370**, 953–962 https://doi.org/10.1042/bj20021476 (2003).
3. Kudryavtseva, E. I. *et al.* Identification and characterization of Grainyhead-like epithelial transactivator (GET-1), a novel mammalian Grainyhead-like factor. *Dev Dyn*, **226**, 604–617 https://doi.org/10.1002/dvdy.10255 (2003).

4. Auden, A. *et al.* Spatial and temporal expression of the Grainyhead-like transcription factor family during murine development. *Gene Expr Patterns*, **6**, 964–970 https://doi.org/10.1016/j.modgep.2006.03.011 (2006).
5. Caddy, J. *et al.* Epidermal wound repair is regulated by the planar cell polarity signaling pathway. *Developmental cell*, **19**, 138–147 https://doi.org/10.1016/j.devcel.2010.06.008 (2010).
6. Kimura-Yoshida, C., Mochida, K., Ellwanger, K., Niehrs, C. & Matsuo, I. Fate Specification of Neural Plate Border by Canonical Wnt Signaling and Grhl3 is Crucial for Neural Tube Closure. *EBioMedicine* **2**, 513–527, doi:10.1016/j.ebiom.2015.04.012 (2015).
7. Alsina, B. & Whitfield, T. T. Sculpting the labyrinth: Morphogenesis of the developing inner ear. *Seminars in Cell & Developmental Biology*, **65**, 47–59 https://doi.org/10.1016/j.semcdb.2016.09.015 (2017).
8. Ting, S. B. *et al.* Inositol- and folate-resistant neural tube defects in mice lacking the epithelial-specific factor Grhl-3. *Nat Med*, **9**, 1513–1519 https://doi.org/10.1038/nm961 (2003).
9. Gustavsson, P. *et al.* Increased expression of Grainyhead-like-3 rescues spina bifida in a folate-resistant mouse model. *Hum Mol Genet*, **16**, 2640–2646 https://doi.org/10.1093/hmg/ddm221 (2007).
10. Ting, S. B. *et al.* A homolog of Drosophila grainy head is essential for epidermal integrity in mice., **308**, 411–413 https://doi.org/10.1126/science.1107511 (2005).
11. Kashgari, G. *et al.* Epithelial Migration and Non-adhesive Periderm Are Required for Digit Separation during Mammalian Development. *Dev. Cell*, **52**, 764–778764 https://doi.org/10.1016/j.devcel.2020.01.032 (2020).
12. Ting, S. B. *et al.* The epidermis of grhl3-null mice displays altered lipid processing and cellular hyperproliferation. *Organogenesis*, **2**, 33–35 https://doi.org/10.4161/org.2.2.2167 (2005).
13. Yu, Z. *et al.* The Grainyhead-like epithelial transactivator Get-1/Grhl3 regulates epidermal terminal differentiation and interacts functionally with LMO4. *Dev Biol*, **299**, 122–136 https://doi.org/10.1016/j.ydbio.2006.07.015 (2006).
14. Darido, C. *et al.* Targeting of the tumor suppressor GRHL3 by a miR-21-dependent proto-oncogenic network results in PTEN loss and tumorigenesis., **20**, 635–648 https://doi.org/10.1016/j.ccr.2011.10.014 (2011).
15. Goldie, S. J. *et al.* Loss of GRHL3 leads to TARC/CCL17-mediated keratinocyte proliferation in the epidermis. *Cell Death Dis*, **9**, 1072 https://doi.org/10.1038/s41419-018-0901-6 (2018).
16. Georgy, S. R. *et al.* Identification of a Novel Proto-oncogenic Network in Head and Neck Squamous Cell Carcinoma. *Journal of the National Cancer Institute*, **107**, https://doi.org/10.1093/jnci/djv152 (2015).
17. Peyrard-Janvid, M. *et al.* Dominant mutations in GRHL3 cause Van der Woude Syndrome and disrupt oral periderm development. *Am J Hum Genet*, **94**, 23–32 https://doi.org/10.1016/j.ajhg.2013.11.009 (2014).

18. Lemay, P. *et al.* Loss-of-function de novo mutations play an important role in severe human neural tube defects. *J Med Genet*, **52**, 493–497 https://doi.org/10.1136/jmedgenet-2015-103027 (2015).
19. Yang, W. *et al.* Genetic variants in GRHL3 and risk for neural tube defects: A case-control and case-parent triad/control study. *Birth Defects Research*, **111**, 1468–1478 https://doi.org/10.1002/bdr2.1556 (2019).
20. De Castro, S. C. P. *et al.* Overexpression of Grainyhead-like 3 causes spina bifida and interacts genetically with mutant alleles of Grhl2 and Vangl2 in mice. *Hum Mol Genet*, **27**, 4218–4230 https://doi.org/10.1093/hmg/ddy313 (2018).
21. Miles, L. B. *et al.* Mis-expression of grainyhead-like transcription factors in zebrafish leads to defects in enveloping layer (EVL) integrity, cellular morphogenesis and axial extension. *Sci. Rep*, **7**, 17607 https://doi.org/10.1038/s41598-017-17898-7 (2017).
22. Kimura-Yoshida, C., Mochida, K., Nakaya, M., Mizutani, T. & Matsuo, I. Cytoplasmic localization of GRHL3 upon epidermal differentiation triggers cell shape change for epithelial morphogenesis. *Nature Communications*, **9**, 4059 https://doi.org/10.1038/s41467-018-06171-8 (2018).
23. Haenebalcke, L. *et al.* Efficient ROSA26-based conditional and/or inducible transgenesis using RMCE-compatible F1 hybrid mouse embryonic stem cells. *Stem Cell Rev Rep*, **9**, 774–785 https://doi.org/10.1007/s12015-013-9458-z (2013).
24. Camerer, E. *et al.* Local protease signaling contributes to neural tube closure in the mouse embryo. *Developmental cell*, **18**, 25–38 https://doi.org/10.1016/j.devcel.2009.11.014 (2010).
25. Silver, L. M. *Mouse genetics: concepts and applications* (Oxford University Press, 1995).
26. Hardman, M. J., Sisi, P., Banbury, D. N. & Byrne, C. Patterned acquisition of skin barrier function during development. *Development*, **125**, 1541 (1998).
27. Cangkrama, M. *et al.* Two Ancient Gene Families Are Critical for Maintenance of the Mammalian Skin Barrier in Postnatal Life. *J Invest Dermatol*, **136**, 1438–1448 https://doi.org/10.1016/j.jid.2016.02.806 (2016).
28. Wilanowski, T. *et al.* Perturbed desmosomal cadherin expression in grainy head-like 1-null mice. *The EMBO journal*, **27**, 886–897 (2008).
29. Deol, M. S. Inherited diseases of the inner ear in man in the light of studies on the mouse. *J Med Genet*, **5**, 137–158 https://doi.org/10.1136/jmg.5.2.137 (1968).
30. Zhou, X., Jen, P. H. S., Seburn, K. L., Frankel, W. N. & Zheng, Q. Y. Auditory brainstem responses in 10 inbred strains of mice. *Brain Res*, **1091**, 16–26 https://doi.org/10.1016/j.brainres.2006.01.107 (2006).
31. Chen, X., Lloyd, S. M., Kweon, J., Gamalong, G. M. & Bao, X. Epidermal progenitors suppress GRHL3-mediated differentiation through intronic polyadenylation promoted by CPSF-HNRNPA3 collaboration. *Nat Commun*, **12**, 448 https://doi.org/10.1038/s41467-020-20674-3 (2021).
32. Kikulska, A. *et al.* Coordinated expression and genetic polymorphisms in Grainyhead-like genes in human non-melanoma skin cancers. *BMC Cancer*, **18**, 23 https://doi.org/10.1186/s12885-017-3943-8 (2018).

33. Mistry, D. S., Chen, Y. & Sen, G. L. Progenitor function in self-renewing human epidermis is maintained by the exosome., **11**, 127–135 https://doi.org/10.1016/j.stem.2012.04.022 (2012).
34. Song, A. J. & Palmiter, R. D. Detecting and Avoiding Problems When Using the Cre–lox System. *Trends in Genetics*, **34**, 333–340 https://doi.org/10.1016/j.tig.2017.12.008 (2018).
35. Spinelli, V. *et al.* Screening strategy to generate cell specific recombination: a case report with the RIP-Cre mice. *Transgenic Res*, **24**, 803–812 https://doi.org/10.1007/s11248-015-9889-1 (2015).
36. Hanakawa, Y., Matsuyoshi, N. & Stanley, J. R. Expression of desmoglein 1 compensates for genetic loss of desmoglein 3 in keratinocyte adhesion. *J Invest Dermatol*, **119**, 27–31 https://doi.org/10.1046/j.1523-1747.2002.01780.x (2002).
37. Hanakawa, Y., Li, H., Lin, C., Stanley, J. R. & Cotsarelis, G. Desmogleins 1 and 3 in the companion layer anchor mouse anagen hair to the follicle. *J Invest Dermatol*, **123**, 817–822 https://doi.org/10.1111/j.0022-202X.2004.23479.x (2004).
38. Peters, L. M. *et al.* Mutation of a transcription factor, TFCP2L3, causes progressive autosomal dominant hearing loss, DFNA28. *Hum Mol Genet*, **11**, 2877–2885 https://doi.org/10.1093/hmg/11.23.2877 (2002).
39. Vona, B., Nanda, I., Neuner, C., Müller, T. & Haaf, T. Confirmation of GRHL2 as the gene for the DFNA28 locus. *Am J Med Genet A*, **161A**, 2060–2065 https://doi.org/10.1002/ajmg.a.36017 (2013).
40. Liu, F. *et al.* Grhl1 deficiency affects inner ear development in zebrafish. *Int J Dev Biol*, **59**, 417–423 https://doi.org/10.1387/ijdb.140230FL (2015).
41. Standring, S. *Gray's anatomy: the anatomical basis of clinical practice* (Forty-first edition. edn, (Elsevier Limited, 2016).
42. Marieb, E. N., Wilhelm, P. B. & Mallatt, J. Human anatomy. Eighth edition. edn(Pearson, 2017).
43. Mangold, E. *et al.* Sequencing the GRHL3 Coding Region Reveals Rare Truncating Mutations and a Common Susceptibility Variant for Nonsyndromic Cleft Palate. *American journal of human genetics*, **98**, 755–762 https://doi.org/10.1016/j.ajhg.2016.02.013 (2016).
44. Miles, L. B., Dworkin, S. & Darido, C. Alternative splicing and start sites: Lessons from the Grainyhead-like family. *Dev. Biol*, **429**, 12–19 https://doi.org/10.1016/j.ydbio.2017.06.018 (2017).
45. Saint-Jeannet, J. P. & Moody, S. A. Establishing the pre-placodal region and breaking it into placodes with distinct identities. *Developmental biology*, **389**, 13–27 https://doi.org/10.1016/j.ydbio.2014.02.011 (2014).
46. Sato, S. *et al.* Conserved expression of mouse Six1 in the pre-placodal region (PPR) and identification of an enhancer for the rostral PPR. *Dev. Biol*, **344**, 158–171 https://doi.org/10.1016/j.ydbio.2010.04.029 (2010).
47. Nyabi, O. *et al.* Efficient mouse transgenesis using Gateway-compatible ROSA26 locus targeting vectors and F1 hybrid ES cells. *Nucleic Acids Res*, **37**, e55 https://doi.org/10.1093/nar/gkp112 (2009).

48. Carpinelli, M. R. *et al.* Inactivation of Zeb1 in GRHL2-deficient mouse embryos rescues mid-gestation viability and secondary palate closure. *Dis Model Mech*, **13**, https://doi.org/10.1242/dmm.042218 (2020).
49. Sakamoto, A., Kuroda, Y., Kanzaki, S. & Matsuo, K. Dissection of the Auditory Bulla in Postnatal Mice: Isolation of the Middle Ear Bones and Histological Analysis. *J Vis Exp*, **55054**, https://doi.org/10.3791/55054 (2017).
50. Ogier, J. M. *et al.* An intronic mutation in Chd7 creates a cryptic splice site, causing aberrant splicing in a mouse model of CHARGE syndrome. *Sci. Rep*, **8**, 5482 https://doi.org/10.1038/s41598-018-23856-8 (2018).

Figures

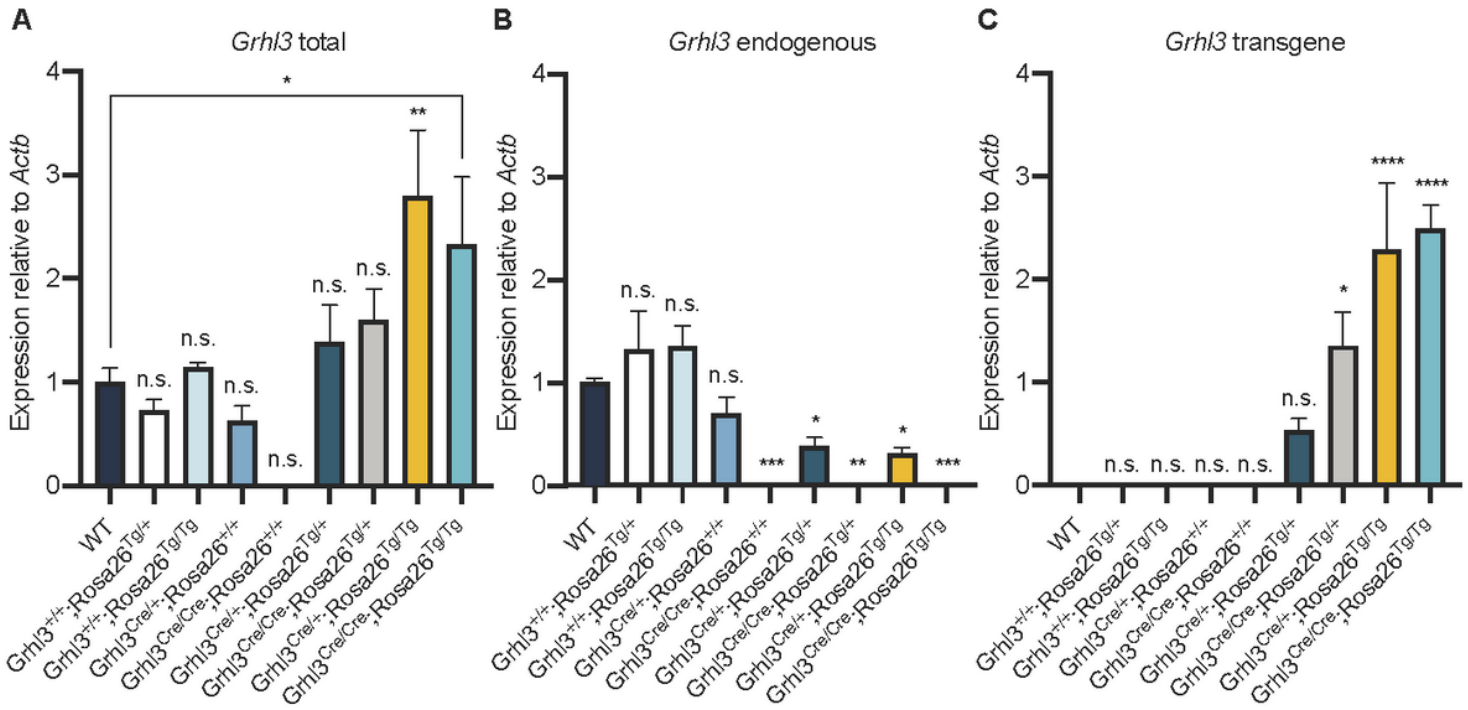

Figure 1

Misexpression of Grhl3 in Grhl3Cre;Rosa26Tg transgenic mouse model. Q-RT-PCR on E18.5 epidermis showing abundance of total Grhl3 mRNA (A), endogenous Grhl3 mRNA (B) and transgene Grhl3 mRNA (C) varies across genotypes. Bar graph presented as a mean ± standard error of mean (SEM). A one-way ANOVA test following by a Dunnett's multiple comparison test between wild-type and other genotypes were used for data analysis. An additional Mann-Whitney test was used to compare the total Grhl3 mRNA level (A) between E18.5 wild-type and Grhl3Cre/Cre;Rosa26Tg/Tg epidermis. * = P-value < 0.05, ** = P-value < 0.01, *** = P-value < 0.001, **** = P-value < 0.00001. n.s., not significant.

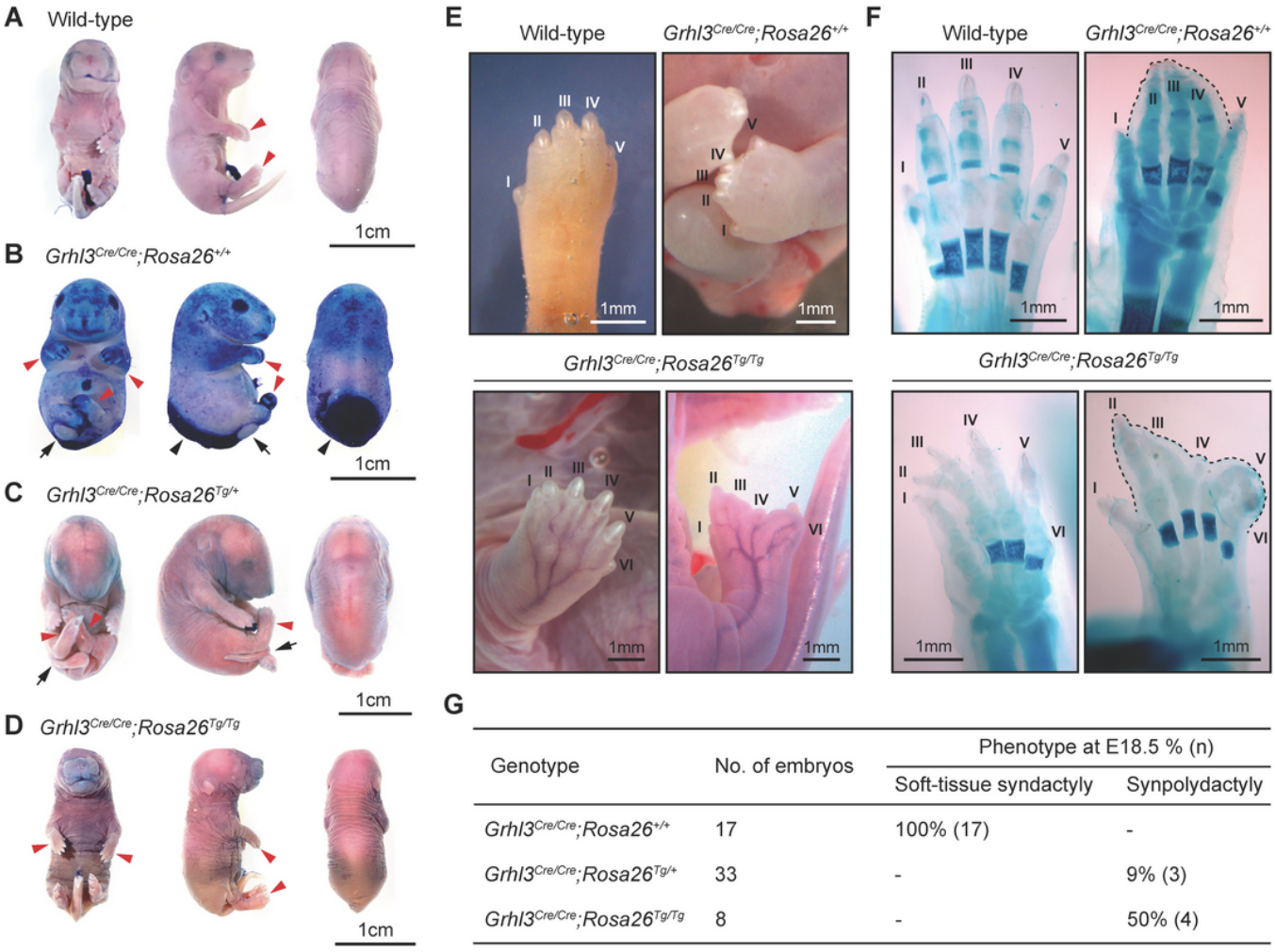

G

Genotype	No. of embryos	Phenotype at E18.5 % (n)	
		Soft-tissue syndactyly	Synpolydactyly
Grhl3$^{Cre/Cre}$;*Rosa26*$^{+/+}$	17	100% (17)	-
Grhl3$^{Cre/Cre}$;*Rosa26*$^{Tg/+}$	33	-	9% (3)
Grhl3$^{Cre/Cre}$;*Rosa26*$^{Tg/Tg}$	8	-	50% (4)

Figure 2

Restoration of Grhl3 expression rescues neurulation and skin barrier defects of Grhl3-null mice while misexpression of Grhl3 expression causes digit defects. (A-D) Skin barrier assay on E18.5 wild-type and transgenic mice. Wild-type embryos (N = 2) showed a fully acquired skin barrier (A). Penetration of toluidine blue into skin indicated impaired skin barrier in Grhl3Cre/Cre;Rosa26+/+ embryos (N = 2). Grhl3Cre/Cre;Rosa26+/+ embryos also showed syndactyly, curly tail and spina bifida (B). Restoration of Grhl3 expression rescued skin barrier defect and spina bifida in Grhl3Cre/Cre;Rosa26Tg/+ embryos (N = 2) (C). Over-expression of Grhl3 in Grhl3Cre/Cre;Rosa26Tg/Tg embryos (N = 2) fully rescued Ghrl3-null phenotypes (D). (E) Gross appearance of digits from wild-type (N = 4), Grhl3Cre/Cre;Rosa26+/+ (N = 4) and Grhl3Cre/Cre;Rosa26Tg/Tg (N = 4) embryos at E18.5. (F) Skeletal preparations of wild-type (N = 4), Grhl3Cre/Cre;Rosa26+/+ (N = 4) and Grhl3Cre/Cre;Rosa26Tg/Tg (N = 2) embryos at E18.5. Grhl3Cre/Cre;Rosa26+/+ embryos exhibited soft-tissue syndactyly. Grhl3Cre/Cre;Rosa26Tg/Tg embryos exhibited synpolydactyly and incompletely formed digits. The dotted line outlines the soft-tissue syndactyly. (G) Penetrance of digit defects among Grhl3Cre/Cre;Rosa26+/+, Grhl3Cre/Cre;Rosa26Tg/+

and Grhl3Cre/Cre;Rosa26Tg/Tg embryos at E18.5. Arrows, curly tail; black arrowheads, spina bifida; red arrowheads, digits.

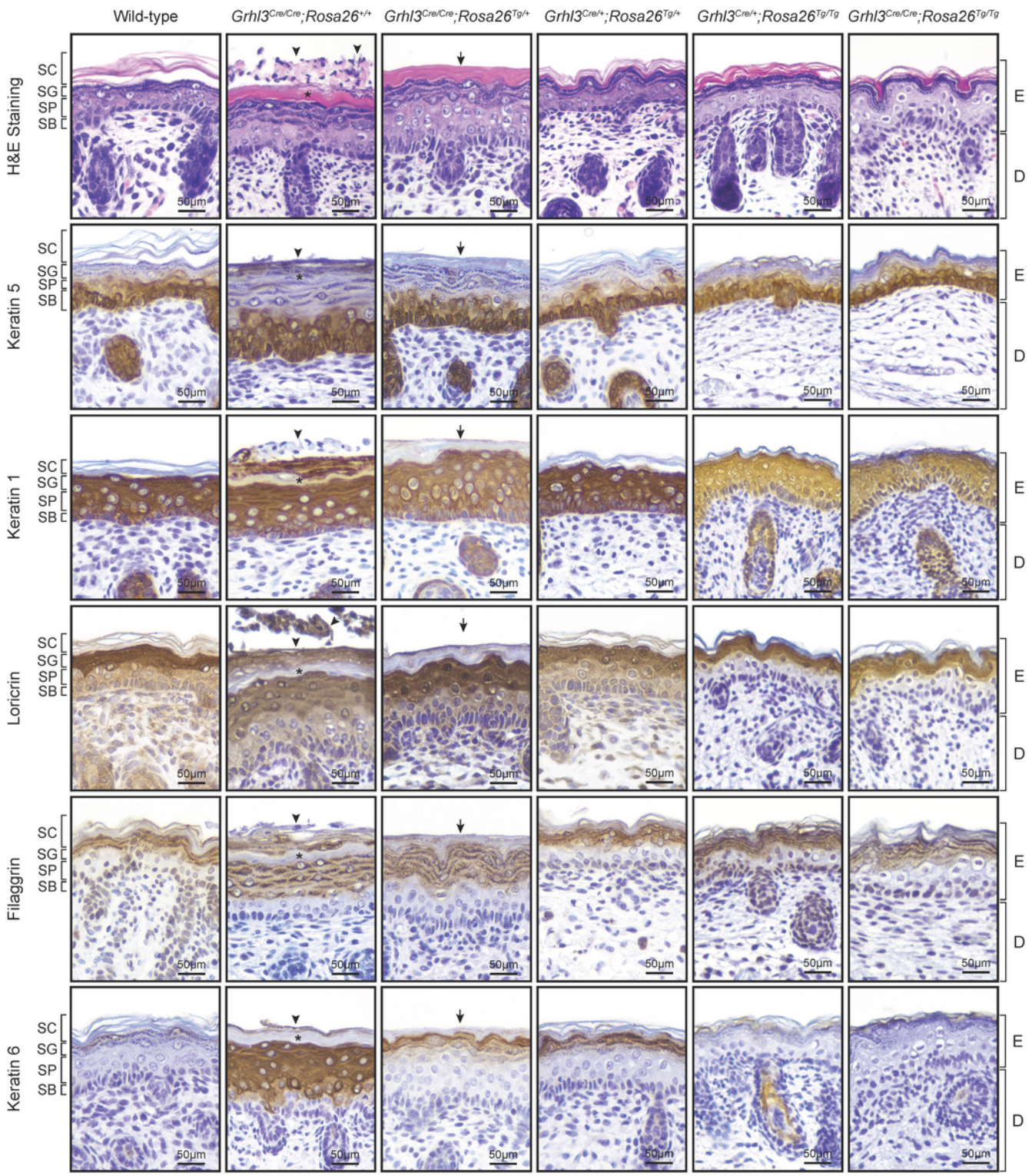

Figure 3

Restoration of Grhl3 expression partially rescues epidermis abnormalities in embryos. Histological and immunostaining analysis of wild-type and transgenic E18.5 epidermis. N = 4. Arrowheads, the extra tissue structure residing superiorly to the epidermis; asterisks, compacted stratum corneum layer between the

extra tissue structure and the stratum granulosum layer; arrows, compacted stratum corneum layer. SC, stratum corneum; SG, stratum granulosum; SP, stratum spinosum; SB, stratum basale; E, epidermis; D, dermis.

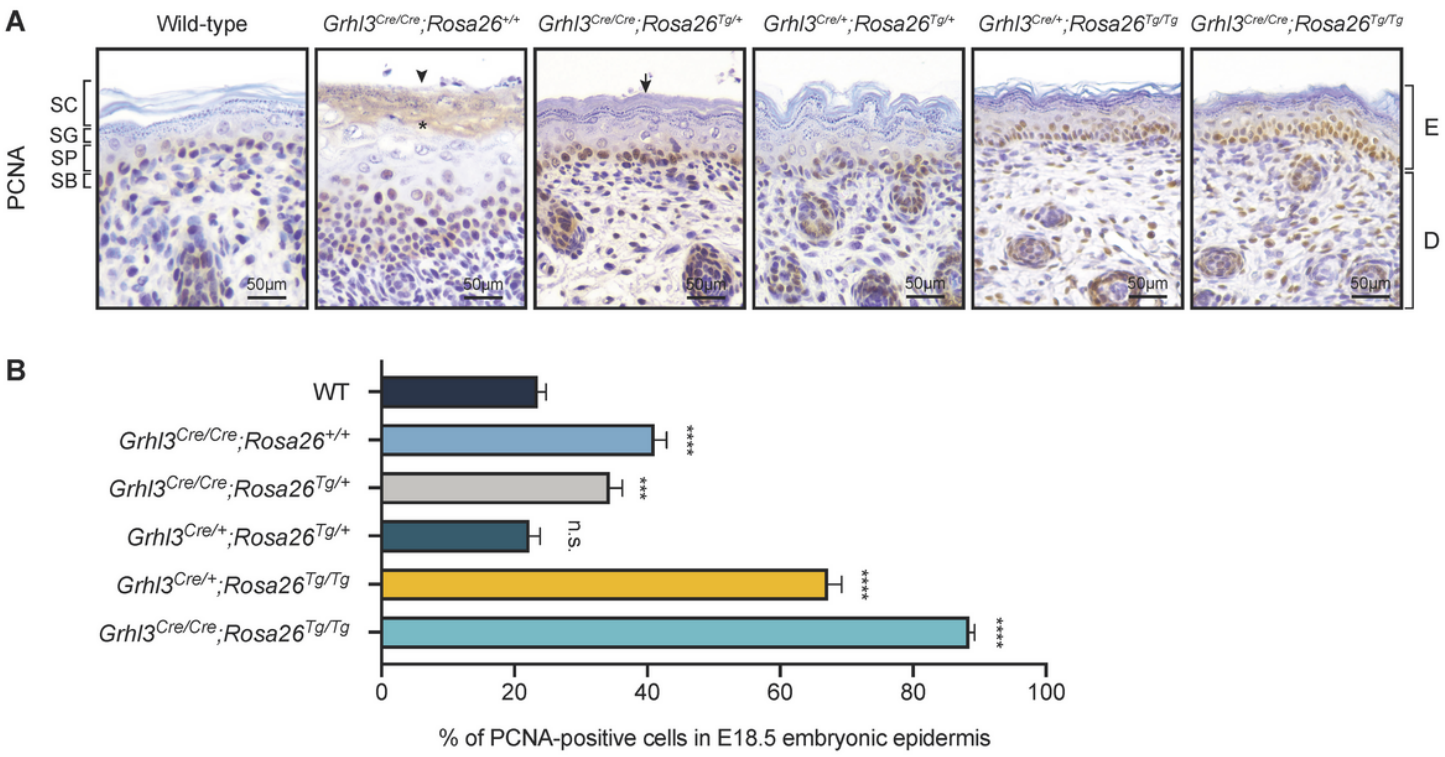

Figure 4

Misexpression of Grhl3 expression leads to basal keratinocyte hyperproliferation. PCNA immunostaining analysis and quantification of PCNA-positive cells in wild-type and transgenic E18.5 epidermis. N = 4. Arrowheads, the extra tissue structure residing superiorly to the epidermis; asterisks, compacted stratum corneum layer between the extra tissue structure and the stratum granulosum layer; arrows, compacted stratum corneum layer. SC, stratum corneum; SG, stratum granulosum; SP, stratum spinosum; SB, stratum basale; E, epidermis; D, dermis. Bar graph presented as a mean ± standard error of mean (SEM). A one-way ANOVA test following by a Dunnett's multiple comparison test between wild-type and other genotypes were used for data analysis. *** = P-value < 0.001, **** = P-value < 0.00001. n.s., not significant.

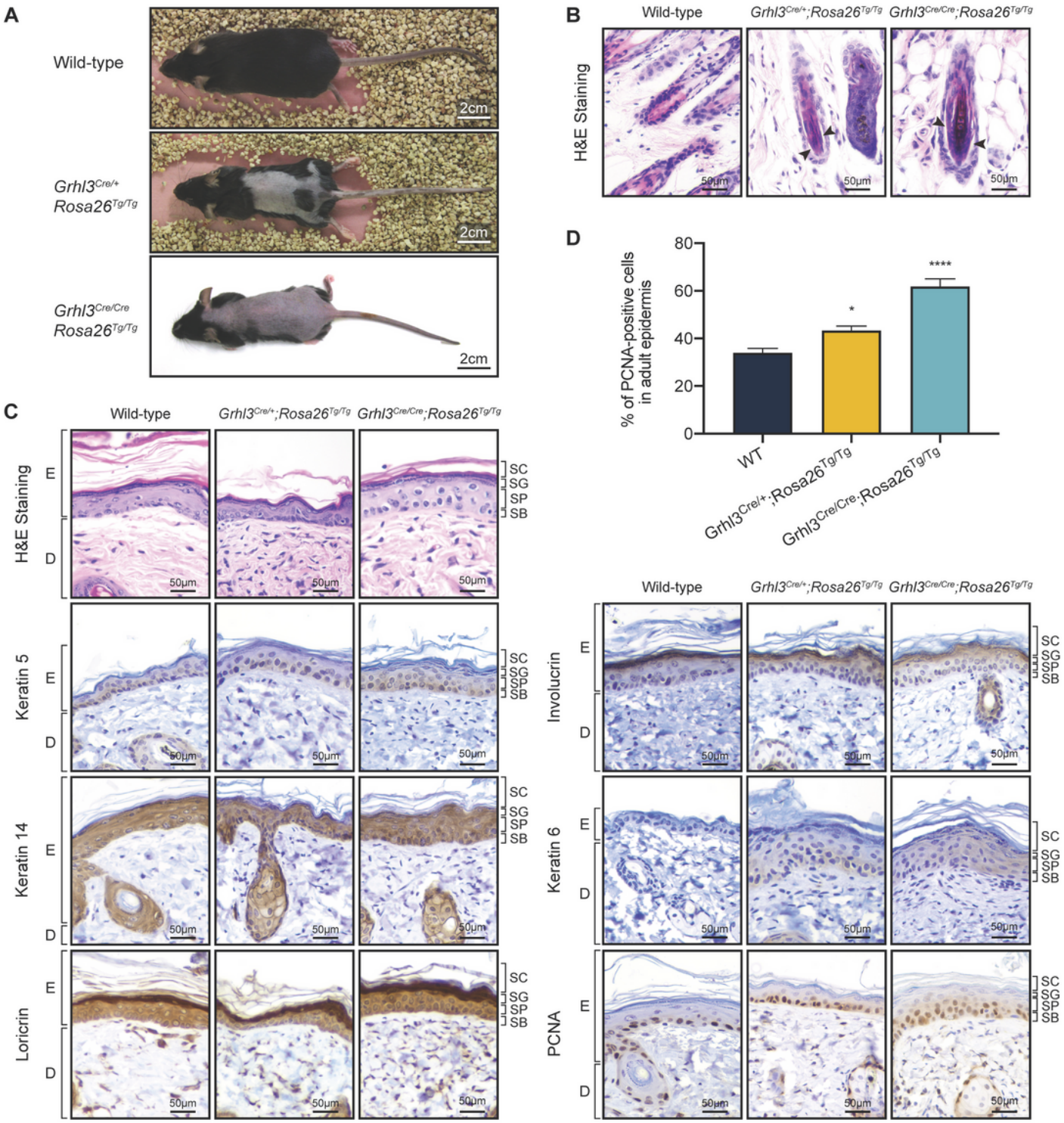

Figure 5

Over-expression of Grhl3 perturbs epidermal homeostasis in adult. (A) Adult Grhl3Cre/+;Rosa26Tg/Tg and Grhl3Cre/Cre;Rosa26Tg/Tg mice displayed large scale of alopecia in the dorsal region (N = 4). (B) Hematoxylin and eosin staining of adult wild-type, Grhl3Cre/+;Rosa26Tg/Tg and Grhl3Cre/Cre;Rosa26Tg/Tg hair follicles (N = 2). (C) Histological and immunostaining analysis of wild-type, Grhl3Cre/+;Rosa26Tg/Tg and Grhl3Cre/Cre;Rosa26Tg/Tg adult epidermis (N = 2). (D) Quantification

of PCNA-positive cells in wild-type, Grhl3Cre/+;Rosa26Tg/Tg and Grhl3Cre/Cre;Rosa26Tg/Tg adult epidermis. Arrowheads, clefts between the inner root sheath and the outer root sheath. SC, stratum corneum; SG, stratum granulosum; SP, stratum spinosum; SB, stratum basale; E, epidermis; D, dermis. Bar graph presented as a mean ± standard error of mean (SEM). A one-way ANOVA test following by a Dunnett's multiple comparison test between wild-type and other genotypes were used for data analysis. * = P-value < 0.05, **** = P-value < 0.00001.

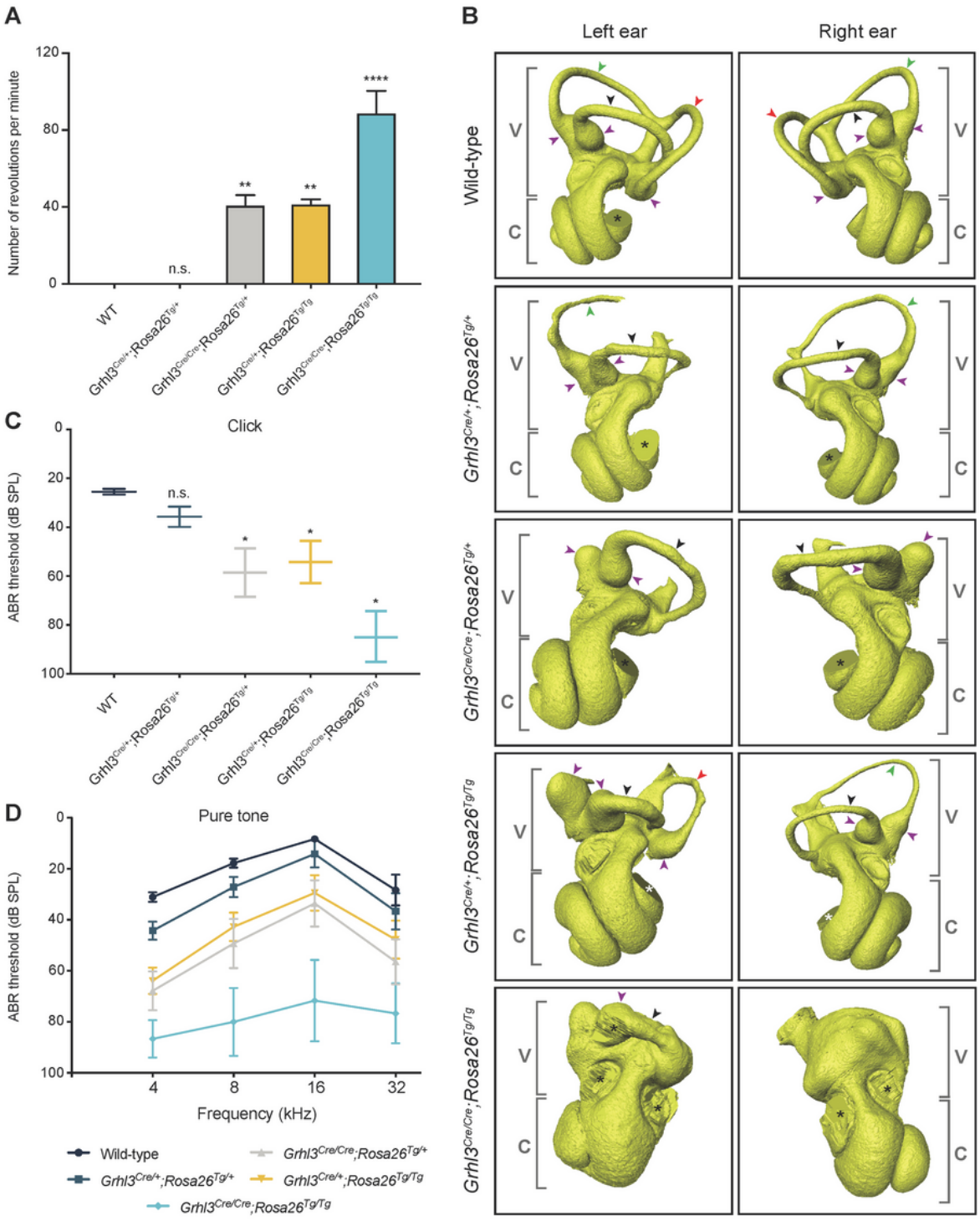

Figure 6

Inner ear malformation and hearing impairment in Grhl3 transgenic mice. (A) Quantification of the number of times that transgenic mice circled per minute (N = 3-4 mice per genotype). (B) 3D reconstructions of the inner ear X-ray micro-computed tomography scanning. (C) Average ABR thresholds of wild-type (N = 10), Grhl3Cre/+;Rosa26Tg/+ (N = 7), Grhl3Cre/Cre;Rosa26Tg/+ (N = 7), Grhl3Cre/+;Rosa26Tg/Tg (N = 7) and Grhl3Cre/Cre;Rosa26Tg/Tg (N = 3) mice when respond to a click containing mixed frequency noise. (D) Average ABR thresholds of wild-type (N = 9), Grhl3Cre/+;Rosa26Tg/+ (N = 7), Grhl3Cre/Cre;Rosa26Tg/+ (N = 7), Grhl3Cre/+;Rosa26Tg/Tg (N = 9) and Grhl3Cre/Cre;Rosa26Tg/Tg (N = 3) mice when respond to pure tone stimuli at 4, 8, 16 and 32 kHz. Black arrowheads, lateral semi-circular canal; green arrowheads, posterior semi-circular canal; red arrowheads, anterior semi-circular canal; purple arrowheads, ampullae; asterisks, artifacts of the scanning and reconstruction. V, vestibular apparatus; C, cochlea. Bar graph and scatter plots presented as a mean ± standard error of mean (SEM). A one-way ANOVA test following by a Dunnett's multiple comparison test between wild-type and other genotypes were used for data analysis. * = P-value < 0.05, ** = P-value < 0.01, **** = P-value < 0.00001. n.s., not significant.

Supplementary Files

This is a list of supplementary files associated with this preprint. Click to download.

- Supplementaryfiles.pdf